Linearity and Calibration of Charge-Division and Rise-Time Encoded Gas PSDs*

R. K. Crawford, P. Thiyagarajan
Argonne National Laboratory, Argonne, IL 60439, USA
J. Chen
Massachusetts Institute of Technology, Cambridge, MA 02139, USA

ABSTRACT

Both linear and area gas proportional counter position-sensitive detectors (PSDs) are used at IPNS, and both charge-division and rise-time encoding schemes are used for these detectors. Impedance mismatching at the detector ends can lead to nonlinearities in the analog portion of the encoding circuits, and digitization errors can lead to local channel-to-channel variations in the position encoding. Some of these nonlinearities can be eliminated by appropriate circuit design, and a calibration scheme has been devised to effectively eliminate the remaining problems. Both the circuit improvements and the calibration methods are discussed.

I. Introduction

Encoding Methods

Figure 1 provides a schematic representation of a one-dimensional position-sensitive detector and preamplifiers. Typical voltage pulses from the preamplifiers are also shown for a neutron detected at a particular position x. In "charge-division encoding" the remainder of the encoding circuitry is designed to determine the peak amplitudes V_A and V_B from the two ends of the detector, and to determine an "encoded position" x' for this event from the relationship

$$x' = \frac{V_B(x)}{V_A(x) + V_B(x)} L_D + x_o \qquad (1)$$

where $L_D = x_B - x_A$ is the detector length, x_A and x_B are the positions of the detector ends, and x_o is a constant which allows adjustment of the encoding offset. Figure 1 also shows the rise times $t_A(x)$ and $t_B(x)$ of the pulses at the two ends of the detector resulting from an event at position x. In "rise-time encoding" the rest of the encoding circuitry determines these "rise times", and the encoded position x' for this event is based on the relationship

$$x' = \frac{L_D}{2}\left[1 - \frac{t_B(x) - t_A(x)}{t_B(x_A) - t_A(x_A)}\right] + x_o \qquad (2)$$

The normalizing constant $t_B(x_A) - t_A(x_A)$, which must be determined empirically, is roughly equal to the "detector time constant" RC, where R and C are the total resistance and capacitance associated with the detector electrode.

* Work supported by U.S. Department of Energy, BES, contract No. W-31-109-ENG-38.

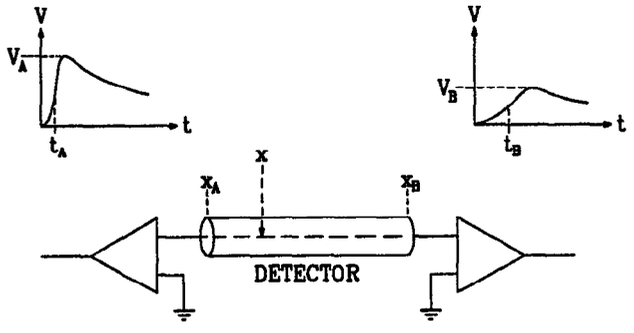

Figure 1. Schematic representation of the charge-division and rise-time encoding schemes.

Linearity Measurements

The linearity of the encoding for position-sensitive detectors can be readily assessed by a "flood pattern" measurement to determine the response of the detector to a uniform flux of neutrons. If N_i is the number of counts measured in the encoded segment i when a detector with detection efficiency ε is under uniform illumination I_o, then

$$N_i = I_o \varepsilon (x_{i+1} - x_i) \tag{3}$$

where x_i and x_{i+1} are the physical positions corresponding to the boundaries of the i^{th} segment and statistical fluctuations have been ignored. Assuming ε is constant, the variation of N_i from segment to segment gives a direct measure of the variation in the ranges of physical detector positions which are mapped into the segments by the encoding process, and hence a direct measure of the differential nonlinearity of the detector encoding.

II. Impedance Mismatching Problems and Solutions

Significant effort has been invested in understanding the position encoding for the PSDs on the GLAD (charge-division encoding) and SAD (rise-time encoding) instruments at IPNS. Figure 2 shows a typical flood pattern measured with one of the GLAD one-dimensional PSDs at an early stage in the development of the charge-division encoding electronics. The large nonlinearities seen near the detector ends affect roughly 20% of the total detector length. In an effort to understand these nonlinearities, the detector was modeled as a uniformly distributed resistance-capacitance (RC) line, and a computer program was used to numerically invert the Laplace transforms for the system comprised of this RC line and its associated analog encoding electronics (charge-sensitive preamplifiers and shaping amplifiers).[1] The calculated pulses at the end of the detector close to the event are large, and show the usual rapid rise to a peak value proportional to the charge collected on the capacitor at that end, followed by a slow decay through the associated discharging resistor. However, for x near either end of the detector, the

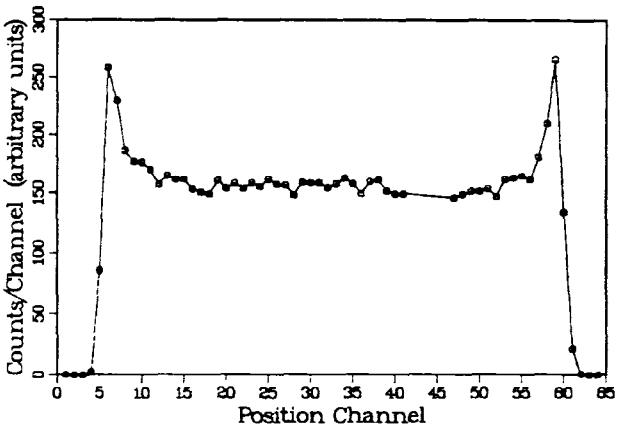

Figure 2. Flood pattern measured with an unterminated GLAD linear PSD.

pulses at the opposite end of the detector are very small, and are distorted from this expected behavior. These small pulses show the rapid rise proportional to the initial charge collected on the capacitor at this end, but this is followed by a substantial additional slow rise due to the discharge of the capacitor at the far end of the detector. While most of that charge is dissipated through the associated resistor, some of it is transferred back through the detector and appears on the capacitor at this end. (This can also be thought of as a "reflection" of part of the initial waveform from the impedance mismatch between the detector and the preamplifier.) The curve labeled "not terminated" in Figure 3 demonstrates this type of behavior. Since the remainder of the electronic circuitry senses the peak of the voltage pulse rather than just the initial rapidly-rising portion, this "double counting" of some of the charge causes the encoded voltage at the end away from the event to be higher than it would be based on the initial charge division alone. This effect disappears rapidly as the event position is moved away from the detector end; analytical expressions have been derived which quantitatively explain this behavior.[1]

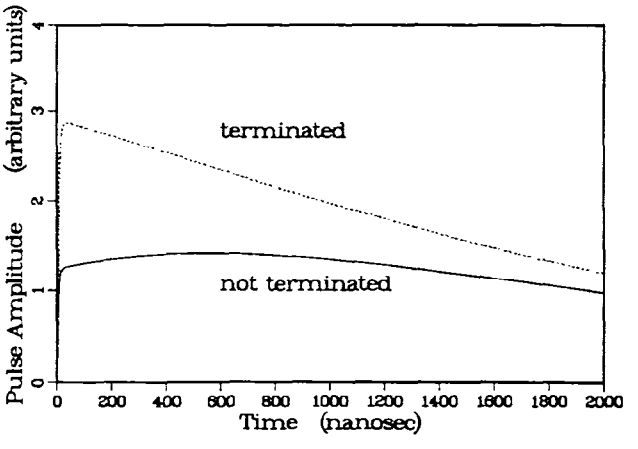

Figure 3. Calculated pulse shape at end B of a GLAD detector for an event at $x=0.05L_D$ in the unterminated and terminated cases.

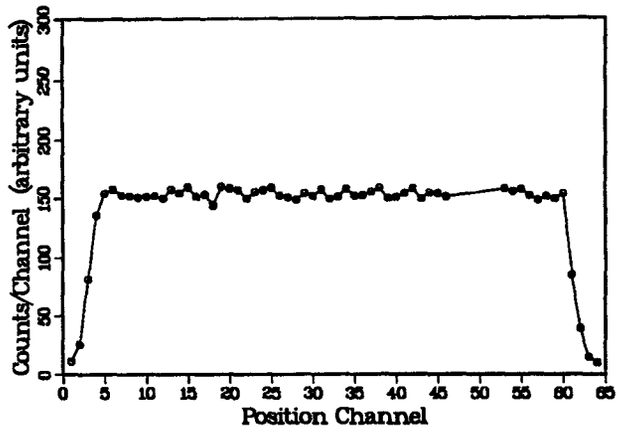

Figure 4. Flood pattern measured for a GLAD detector after the termination was added.

These calculations made clear a number of changes to the encoding circuitry which would partially or entirely alleviate the problem. These included using preamplifiers with much higher open-loop gain, using very fast pulse shaping electronics to filter out the slow-rising component, and simply adding small terminating resistors to the ends of the detector. In this latter procedure, which was adopted for the GLAD detectors, these resistors appear to the circuit as neutronically-inactive extensions of the detector. Then since the active regions of the "modified detector" are all farther away from the effective electronic ends of the modified detector, all the active regions fall within the portion where the encoding is linear. The curve labeled "terminated" in Figure 3 shows the calculated voltage pulse under these conditions, and indicates that while there is still some distortion of the pulse at the end away from the event, this distortion affects only the long-time portion of the pulse shape and does not affect the peak value. Figure 4 shows the almost completely linear flood pattern measured for a GLAD detector which has had such resistors added.

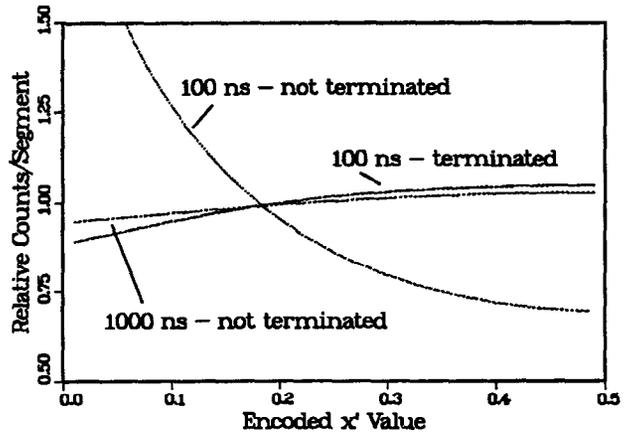

Figure 5. Calculated flood patterns for rise-time encoding with different pulse shaping times and different types of termination. Because of symmetry, only half of the detector is shown. L_D=1 in this example.

Impedance-matching also plays an important role in the linearity of rise-time encoding, but the mechanism is much more complicated than in the case of charge-division encoding. Figure 5 shows one-dimensional flood patterns calculated for a rise-time encoded PSD, using pulse-shaping time-constants of 100 ns and 1000 ns for the analog portion of the of encoding electronics. System parameters for the calculations were chosen to match those of the 20 x 20 cm^2 two-dimensional rise-time-encoded PSD used on SAD. The figure shows considerable nonlinearity, with better linearity when longer time constants are used. This behavior is also seen in flood patterns measured on the SAD detector, and is consistent with the empirically-determined linearity rules of Borkowski and Kopp.[2] However, the calculations also indicate that with properly chosen resistance-capacitance termination networks at the ends of the detector electrodes, the detector encoding can be made essentially linear while using much shorter pulse-shaping time constants. Calculations for such a "terminated" configuration with a shaping time constant of 100 ns are also shown in the figure, where it can be seen that in this "terminated" case the linearity is nearly as good with the shorter time constant as it was with the much longer time constant in the "not terminated" case. Since the shorter time constants permit operation at higher data rates, such termination networks may be a useful addition to the detector electronics.

IV. Digitization Problems

Close inspection of Figs. 2 or 4 shows significant segment-to-segment variations in the encoded flood patterns for the GLAD detectors. These variations are systematic, and far exceed the expected statistical fluctuations. These are a result of the nonlinearities in the charge-division-encoding digitization circuitry, and are generally different for every different set of digitization electronics, and hence for every detector. It has not been possible to eliminate such variations without resorting to much more expensive circuitry. However, the calibration procedures discussed below can correct for these variations as well as for the segment-to-segment variations sometimes associated with the digitization process for rise-time encoding.

V. Calibration Methods and Correction Algorithms

We have developed a procedure, valid for both charge-division and rise-time encoded data, for correcting for any remaining nonlinearities in the encoded data.[3] Consider a one-dimensional PSD which has been binned into n spatial segments. In the analog portion of the encoding process, an event occurring at position x will be encoded to have occurred at x' with a probability given by the resolution function P(x,x'). If the incident intensity per unit length is $I_o(x)$ and the detection efficiency is ε, then the measured intensity will be I(x') given by

$$I(x') = \varepsilon \int_{-\infty}^{\infty} I_o(x) P(x,x') dx \qquad (4)$$

The number of counts N_i recorded for segment i is just

$$N_i = \int_{x_i}^{x_{i+1}} I(x')dx' \tag{5}$$

If we assume that the resolution function is gaussian with standard deviation σ and that the illumination intensity has the uniform value I_o over the length of the detector, then this becomes

$$N_i = \frac{I_o\varepsilon}{\sqrt{2\pi}} \int_{x_i}^{x_{i+1}} \int_{x_A}^{x_B} \frac{1}{\sigma(x)} e^{-(x-x')^2/2\sigma^2(x)}\, dx\, dx' \tag{6}$$

In the case of infinitely sharp resolution ($\sigma = 0$), Eq. (6) reduces to

$$N_i = \left\{ \begin{array}{rll} 0 & \text{for} & x_i < x_{i+1} < x_A \\ I_o\varepsilon(x_{i+1} - x_A) & \text{for} & x_i < x_A < x_{i+1} \\ I_o\varepsilon(x_{i+1} - x_i) & \text{for} & x_A < x_i < x_{i+1} < x_B \\ I_o\varepsilon(x_B - x_i) & \text{for} & x_i < x_B < x_{i+1} \\ 0 & \text{for} & x_B < x_i < x_{i+1} \end{array} \right\} \tag{7}$$

If the encoded positions are accurately known for two physical positions, say x_α and x_β, which are a distance L apart, then

$$I_o\varepsilon = \frac{1}{L} \sum_{x_i=x_\alpha}^{x_i=x_\beta} N_i \tag{8}$$

where some interpolation may be required to handle the end segments in the sum. If one of these known positions is then used to find one of the x_i (by interpolation to the end of the corresponding segment), then Eq. (7) can be used to find all of the other x_i in terms of the N_i from the flood pattern. If all of the intensity from the ends of the detector is recorded in the flood pattern data, then x_A and x_B can be determined from the conservation of intensity, as

$$x_A = x_\alpha - \frac{1}{I_o\varepsilon} \sum_{x<x_\alpha} N_i \tag{9}$$

$$x_B = x_\alpha + \frac{1}{I_o\varepsilon} \sum_{x>x_\alpha} N_i \tag{10}$$

If the resolution $\sigma(x)$ is not infinitely small, but can be assumed to vary only slowly with x (the usual case), then it can be replaced with $\sigma(x')$ in the integral in Eq. (6). In regions of the

detector which are several σ from the ends, the limits of integration x_A to x_B in Eq. (6) can be replaced with $-\infty$ to $+\infty$, and the integral over x can be evaluated to give

$$N_i = I_o \varepsilon \int_{x_i}^{x_{i+1}} dx' = I_o \varepsilon (x_{i+1} - x_i) \qquad \text{for} \quad x_A << x << x_B \tag{11}$$

which is independent of the value of σ and is equivalent to Eq. (7). Thus resolution effects can be ignored for the central portion of the flood pattern, and the procedure outlined above with Eqs. (7) and (8) can still be used for calibration of the central portion of the detector.

Near the ends x_A and x_B of the detector, the resolution must be taken explicitly into account in Eq. (6). For segments near end A, x_B can be replaced by $+\infty$ as the limit of integration, giving

$$N_i = \frac{I_o \varepsilon}{\sqrt{2\pi}} \int_{x_i}^{x_{i+1}} \frac{1}{\sigma(x')} \int_{x_A}^{\infty} e^{-(x-x')^2/2\sigma^2(x')} \, dx \, dx'$$

$$= \frac{I_o \varepsilon}{2} (x_{i+1} - x_i) + \frac{I_o \varepsilon}{2} \int_{x_i}^{x_{i+1}} \operatorname{erf}\left(\frac{x' - x_A}{\sqrt{2}\sigma} \right) dx' \tag{12}$$

This equation can be solved for x_i if x_{i+1} is known, so it is only necessary to start at a point where x_{i+1} is known from Eq. (7) and then solve Eq. (12) repetitively for successively smaller values of i. A similar procedure can be used for calibration near end B. Equations (9) and (10) can still be used to determine x_A and x_B in this case.

For most area detectors, the encoding of the x and y positions is done independently, so the calibration procedure involves such a one-dimensional calibration in each dimension. Figure 6 shows a uniform-illumination flood pattern for the SAD area detector. Separate measurements made with a mask in front of the detector were least-squares fit to determine the local values of $\sigma(x)$ and $\sigma(y)$, and the encoded x' and y' values for the known x and y coordinates of the center of each hole in the mask. These values were used for x_α and x_β (and also for y_α and y_β), and the above procedure was applied to the data of Fig. 6 (averaged over the central portion of the detector) to determine the set of $\{x_i\}$ and $\{y_j\}$. Once these boundaries of each encoded segment of the detector were known, the data from the original pattern could be corrected to determine the "true" resolution-broadened efficiency-weighted intensity pattern $I(x,y)\varepsilon$ according to

$$I_{i,j}(x,y)\varepsilon = \frac{N_{i,j}}{(x_{i+1} - x_i)(y_{j+1} - y_j)} \tag{13}$$

Figure 7 shows the data of Fig. 6 corrected to produce I(x,y) in this manner. This procedure has proven to be quite satisfactory, and is now used for much of the data collected on SAD.

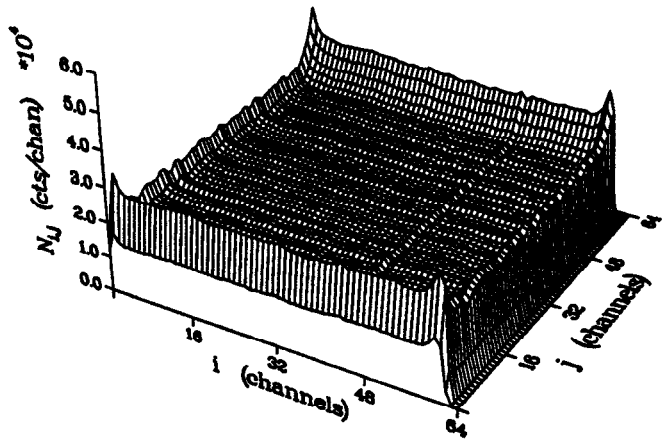

Figure 6. Measured flood pattern for the rise-time encoded detector used on SAD.

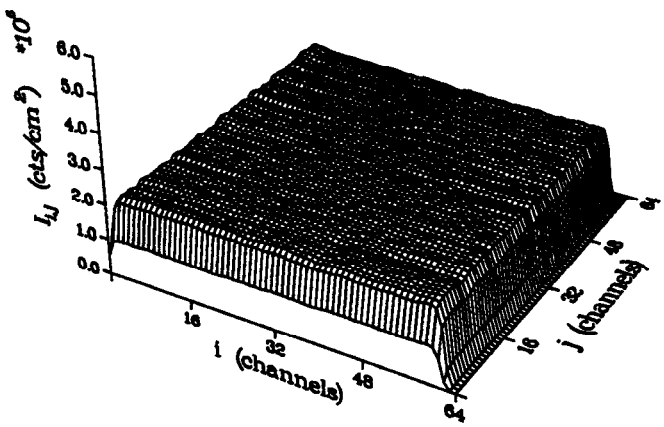

Figure 7. Flood pattern of Fig. 6 corrected for detector nonlinearities by the method discussed in the text.

References

1. R. K. Crawford and J. R. Haumann. *Nucl. Instrum. Meth.* **A292**, 656-670 (1990).
2. C. J. Borkowski and M. K. Kopp. *Rev. Sci. Instrum.* **46**, 951-962 (1975).
3. P. Thiyagarajan, K. F. Bradley, R. K. Crawford, J. E. Epperson, D. G. Wozniak and J. M. Carpenter. Proceedings of SPIE's 1992 International Symposium on Optical Applied Science and Engineering, San Diego, Calif., July 19-23, 1992, Vol. 1737, pp. 243-254.